

---

# Neural Lyapunov Control for Discrete-Time Systems

---

Junlin Wu<sup>1</sup> Andrew Clark<sup>1</sup> Yiannis Kantaros<sup>1</sup> Yevgeniy Vorobeychik<sup>1</sup>

## Abstract

While ensuring stability for linear systems is well understood, it remains a major challenge for systems with nonlinear dynamics. A general approach in such cases is to leverage Lyapunov stability theory to compute a combination of a Lyapunov control function and an associated control policy. However, finding Lyapunov functions for general nonlinear systems is a challenging task. To address this challenge, several methods have been recently proposed that represent Lyapunov functions using neural networks. However, such approaches have been designed exclusively for continuous-time systems. We propose the first approach for learning neural Lyapunov control in discrete-time systems. Three key ingredients enable us to effectively learn provably stable control policies. The first is a novel mixed-integer linear programming approach for verifying the stability conditions in discrete-time systems. The second is a novel approach for computing sub-level sets which characterize the region of attraction. Finally, we rely on a heuristic gradient-based approach for quickly finding counterexamples to significantly speed up Lyapunov function learning. Our experiments on four standard benchmarks demonstrate that our approach significantly outperforms state-of-the-art baselines. For example, on the path tracking benchmark, we outperform recent neural Lyapunov control baselines by an order of magnitude in both running time and the size of the region of attraction, and on two of the four benchmarks (cartpole and PVTOL), ours is the first automated approach to return a provably stable controller.

## 1. Introduction

Stability analysis for dynamical systems aims to show that the system state will stay close and return to an equilibrium under small perturbations. Designing stable control in nonlinear systems commonly relies on constructing Lyapunov functions that can certify the stability of equilibrium points and estimate their region of attraction. However, finding Lyapunov functions for arbitrary nonlinear systems is a challenging task that requires substantial expertise and manual effort (Khalil, 2015). To address this challenge, recent progress has been made in learning Lyapunov functions in *continuous-time* nonlinear dynamics (Abate et al., 2020; Chang et al., 2019; Zhou et al., 2022). However, few approaches exist for doing so in discrete-time systems (Dai et al., 2021), and none for general Lipschitz-continuous dynamics. Since modern learning-based controllers often take non-negligible time for computation, the granularity of control is effectively discrete-time, and developing approaches for stabilizing such controllers is a major open challenge.

We propose a novel method to learn Lyapunov functions and stabilizing controllers, represented as neural networks (NNs) with ReLU activation functions, for discrete-time nonlinear systems. The proposed framework consists of a *learner*, which uses a gradient-based method for updating the parameters of the Lyapunov function and policy, and a *verifier*, which produces counterexamples (if any exist) to the stability conditions that are added as training data for the learner. The use of a verifier in the learning loop is critical to enable the proposed approach to return a provably stable policy. However, no prior approaches enable sound verification of neural Lyapunov stability for general discrete-time dynamical systems. The closest is Dai et al. (2021), who assume that dynamics are represented by a neural network, an assumption that rarely holds in real systems. To address this gap, we develop a novel verification tool that checks if the candidate NN Lyapunov function satisfies the Lyapunov conditions by solving Mixed Integer Linear Programs (MILPs). This approach can soundly verify a broad class of dynamical system models. However, using a sound verification tool in the learning loop makes it a significant bottleneck, severely limiting scalability. We address this problem by also developing a highly effective gradient-based

---

<sup>1</sup>Department of Computer Science and Engineering, Washington University in St. Louis, St. Louis, MO, USA. Correspondence to: Junlin Wu <junlin.wu@wustl.edu>.

technique for identifying counterexamples, resorting to the full MILP-based verifier only as a last resort. The full learning process thereby iterates between learning and verification steps, and returns only when the sound verifier is able to prove that the Lyapunov function and policy satisfy the stability conditions.

We evaluate the proposed approach in comparison to state-of-the-art baselines on four standard nonlinear control benchmarks. On the two simpler domains (inverted pendulum and path following), our approach outperforms the state-of-the-art continuous-time neural Lyapunov control approaches by at least several factors and up to an order of magnitude *in both running time and the size of the region of attraction*. On the two more complex domains—cartpole and PVTOL—ours *is the first automated approach that returns a provably stable controller*.

In summary, we develop (1) a new approach for verifying discrete-time controlled nonlinear systems using mixed-integer linear programming, (2) the first method for learning provably stabilizing controllers for a broad class of discrete-time nonlinear systems; and (3) extensive experiments on four standard benchmarks demonstrating that our approach significantly outperforms prior art.

**Related work** Much prior work on learning Lyapunov functions has focused on continuous-time systems (Abate et al., 2020; Ravanbakhsh & Sankaranarayanan, 2019; Chang et al., 2019; Zhou et al., 2022). Common approaches in the past have assumed that dynamics are linear (Donti et al., 2021; Tedrake, 2009) or polynomial (Ravanbakhsh & Sankaranarayanan, 2019). Recently, Chang et al. (2019), Rego & de Araújo (2022), and Zhou et al. (2022) proposed learning Lyapunov functions represented as neural networks while restricting policies to be linear. These were designed for continuous-time dynamics, and are not effective in discrete-time settings, as we show in the experiments. Chen et al. (2021a) learns convex Lyapunov functions for discrete-time hybrid systems. Their approach requires hybrid systems to admit a mixed-integer linear programming formulation, essentially restricting it to piecewise-affine systems, and does not learn stabilizing controllers for these. Our approach considers a much broader class of dynamical system models, and learns provably stable controllers and Lyapunov functions, allowing both to be represented as neural networks. Kolter & Manek (2019) learn stable nonlinear dynamics represented as neural networks, but do not provide stability guarantees with respect to the true underlying system. In addition, several approaches have been proposed that either provide only probabilistic stability guarantees (Berkenkamp et al., 2017; Richards et al., 2018), or do not guarantee stability (Choi et al., 2020; Han et al., 2020). Several recent approaches propose methods for verifying stability in dynamical discrete-time systems. Chen et al. (2021b) compute an approximate region of attraction of dynamical systems with neural network dynamics, but assume that Lyapunov functions are quadratic. Dai et al. (2021) consider the problem of verifying Lyapunov conditions in discrete-time systems, as well as learning provably stable policies. However, they assume that dynamics are represented by neural networks with (leaky) ReLU activation functions. Our verification approach, in contrast, is for arbitrary Lipschitz continuous dynamics.

## 2. Problem Formulation

We consider a discrete-time nonlinear dynamical system

$$x_{t+1} = f(x_t, u_t), \quad (1)$$

where  $x_t \in \mathcal{X}$  is state in a domain  $\mathcal{X}$  and  $u_t$  the control input at time  $t$ . We assume that  $f$  is Lipschitz continuous. This class of dynamical systems includes the vast majority of (non-hybrid) dynamical system models in prior literature. Following conventional setup, we suppose that  $x = 0$  is an equilibrium point for the system, that is,  $f(0, u) = 0$  for some  $u$ . Let  $\pi(x)$  denote a control policy, with  $u_t = \pi(x_t)$ . For example, in autonomous vehicle path tracking,  $x$  can measure path tracking error and  $u$  the steering angle. Our goal is to learn a control policy  $\pi$  such that the dynamical system in Equation (1) converges to the equilibrium  $x = 0$ , a condition referred to as *stability*. To this end, we leverage the Lyapunov stability framework (Tedrake, 2009). Specifically, our goal is to identify a Lyapunov function  $V(x)$  and controller  $\pi$  that satisfies the following conditions over a subset of the domain  $\mathcal{R} \subseteq \mathcal{X}$  (we refer to  $\mathcal{R}$  as the *valid region*):

$$V(0) = 0 \quad (2a)$$

$$V(x) > 0 \quad \forall x \in \mathcal{R} \setminus \{0\} \quad (2b)$$

$$V(f(x, \pi(x))) - V(x) < 0 \quad \forall x \in \mathcal{R}. \quad (2c)$$

These conditions imply that the system is (locally) stable in the Lyapunov sense (Tedrake, 2009).

What we are ultimately interested in is to obtain a large *region of attraction (ROA)*, defined as the largest set  $\mathcal{R} \subseteq \mathcal{X}$  such that  $\lim_{t \rightarrow \infty} x_t = 0$  for all  $x_0 \in \mathcal{R}$  and  $x_{t+1} = f(x_t, \pi(x_t))$ . Since ROA can have an extremely complex shape, a means

to obtain a set within an ROA that has this desirable property is via *sub-level sets*  $\{x \in \mathcal{R} \mid V(x) < \rho\}$  parameterized by  $\rho > 0$ .

We assume that the Lyapunov function as well as the policy can be represented in a parametric function class, such as by a deep neural network. Formally, we denote the parametric Lyapunov function by  $V_\theta(x)$  and the policy by  $\pi_\beta(x)$ , where  $\theta$  and  $\beta$  are their respective parameters. Our goal is to learn  $V_\theta$  and  $\pi_\beta$  that *provably* satisfy the conditions (2) over as large valid region  $\mathcal{R}$  as possible. This, in turn, enables us to identify an associated ROA. To add structure to the problem, we consider valid regions of the following form:  $\mathcal{R}(\gamma) = \{x \in \mathcal{X} \mid \|x\|_\infty \leq \gamma\}$ . As long as the domain is bounded, a sufficiently large  $\gamma$  yields  $\mathcal{R} = \mathcal{X}$ . Additionally, define  $\mathcal{D}(\gamma)$  as the set of all combinations of  $\theta$  and  $\beta$  for which the conditions (2) are satisfied over the domain  $\mathcal{R}(\gamma)$ . The key challenge in this problem is to find  $(\theta, \beta) \in \mathcal{D}(\gamma)$  for a given  $\gamma$ , that is, to find the parameters of the Lyapunov control function and policy that provably satisfy the conditions (2). That, in turn, entails solving the key subproblem of verifying these conditions for given  $V_\theta$  and  $\pi_\beta$ .

Next, we begin by addressing the verification problem, and then describe our approach for jointly learning  $V_\theta$  and  $\pi_\beta$  that can be verified to satisfy the Lyapunov conditions for a given  $\mathcal{R}(\gamma)$ .

### 3. Verifying Lyapunov Conditions

Prior work on learning Lyapunov functions for continuous-time nonlinear control problems has leveraged off-the-shelf SMT solvers, such as dReal (Gao et al., 2013). However, these solvers scale poorly in our setting (e.g., a single verification for discrete-time PVTOL in Section 5 using dReal fails to return a result within 24 hours). In this section, we propose a novel approach for verifying the Lyapunov conditions for arbitrary Lipschitz continuous dynamics using mixed-integer linear programming by obtaining piecewise-linear bounds on the dynamics, where we assume that  $V_\theta$  and  $\pi_\beta$  are  $K$ - and  $N$ -layer neural networks, respectively, with ReLU activations.

We begin with the simpler problem of verifying constraint (2b). Note that since  $V$  is piecewise linear, it can be solved using MILP through linearization in standard ways (Bertsimas & Tsitsiklis, 1997). Specifically, we formulate this as the following feasibility problem:

$$z_K \leq 0 \tag{3a}$$

$$z_{l+1} = g_{\theta_l}(z_l), \quad 0 \leq l \leq K-1 \tag{3b}$$

$$\|x\|_\infty \leq \gamma, \quad z_0 = x, \tag{3c}$$

where  $l$  refers to a layer in the neural network  $V_\theta$ ,  $z_K = V_\theta(x)$ , and the associated functions  $g_{\theta_l}(z_l)$  are either  $W_l z_l + b_l$  for a linear layer (with  $\theta_l = (W_l, b_l)$ ) or  $\max\{z_l, 0\}$  for a ReLU activation.<sup>1</sup> Any feasible solution  $x^*$  is then a counterexample, and if the problem is infeasible, the condition is satisfied. ReLU activations  $g(z)$  can be linearized by introducing an integer variable  $a \in \{0, 1\}$ , and replacing the  $z' = g(z)$  terms with constraints  $z' \leq Ua$  and  $z' \leq -L(1-a)$ , where  $L$  and  $U$  are specified so that  $L \leq z \leq U$  (we return to the problem of identifying  $L$  and  $U$  below).

Next, we cast verification of constraint (2c) which involves the nonlinear control dynamics  $f$  as the following feasibility problem:

$$\bar{z}_K - z_K \geq -\zeta \tag{4a}$$

$$y_{i+1} = h_{\beta_i}(y_i), \quad 0 \leq i \leq N-1 \tag{4b}$$

$$\bar{z}_{l+1} = g_{\theta_l}(\bar{z}_l), \quad 0 \leq l \leq K-1 \tag{4c}$$

$$\bar{z}_0 = f(x, y_N) \tag{4d}$$

$$y_0 = x, \quad \text{constraints (3b) - (3c)}, \tag{4e}$$

where  $h_{\beta_i}(\cdot)$  are functions computed at layers  $l$  of  $\pi_\beta$ ,  $\zeta > 0$  is a small constant,  $z_K = V_\theta(x)$ , and  $\bar{z}_K = V_\theta(f(x, \pi_\beta(x)))$ . Again, a feasible solution  $x^*$  is a counterexample, while existence of no solution implies that this Lyapunov condition is satisfied.

At this point, all of the constraints can be linearized as before with the exception of Constraint (4d), which involves the nonlinear dynamics  $f$ . To deal with this, we relax the verification problem by replacing  $f$  with linear lower and upper bounds. To obtain tight bounds, we divide  $\mathcal{R}(\gamma)$  into a collection of subdomains  $\{\mathcal{R}_k\}$ . For each  $\mathcal{R}_k$ , we obtain a linear

<sup>1</sup>As in SMT-based verification, we also add a constraint that  $\|x\|_\infty \geq \epsilon$  for a small  $\epsilon$  to avoid numerical instability close to the origin.

lower bound  $f_{lb}(x)$  and upper bound  $f_{ub}(x)$  on  $f$ , and relax the problematic Constraint (4d) into  $f_{lb}(x) \leq \bar{z}_0 \leq f_{ub}(x)$ , which is now a pair of linear constraints. We can then solve Problem (4) for each  $\mathcal{R}_k$ .

**Computing Linear Bounds on System Dynamics** Recall that  $f : \mathbb{R}^n \mapsto \mathbb{R}^n$  is the Lipschitz-continuous system dynamic  $x_{t+1} = f(x_t, u_t)$ . Let  $\lambda$  be the  $\ell_\infty$  Lipschitz constant of  $f$ . Suppose that we are given a region of the domain  $\mathcal{R}_k$  represented as a hyperrectangle, i.e.,  $\mathcal{R}_k = \times_i [x_{i,l}, x_{i,u}]$ , where  $[x_{i,l}, x_{i,u}]$  are the lower and upper bounds of  $x$  along coordinate  $i$ . Our goal is to compute a linear upper and lower bound on  $f(x)$  over this region. We bound  $f_j(x) : \mathbb{R}^n \mapsto \mathbb{R}$  along each  $j$ -th dimension separately. By  $\lambda$ -Lipschitz-continuity, we can obtain  $f_j(x) \leq f_j(x_{1,l}, x_{2,l}, \dots, x_{n,l}) + \lambda \sum_i (x_i - x_{i,l})$  and  $f_j(x) \geq f_j(x_{1,l}, x_{2,l}, \dots, x_{n,l}) - \lambda \sum_i (x_i - x_{i,l})$ . The full derivation is provided in the Supplement Section B.

Alternatively, if  $f_j$  is differentiable, convex over  $x_i$ , and monotone over other dimensions, we can restrict it to calculating one-dimensional bounds by finding  $x_{-i,u}$  and  $x_{-i,l}$  such that  $f_j(x_i, x_{-i,l}) \leq f_j(x_i, x_{-i}) \leq f_j(x_i, x_{-i,u})$  for any given  $x$ , then  $f_j(x) \leq f_{j,i,ub}(x) \equiv f_j(x_{i,l}, x_{-i,u}) + \frac{f_j(x_{i,u}, x_{-i,u}) - f_j(x_{i,l}, x_{-i,u})}{x_{i,u} - x_{i,l}} (x_i - x_{i,l})$  and  $f_j(x) \geq f_{j,i,lb}(x) \equiv f_j(x_i^*, x_{-i,l}) + f'_j(x_i^*, x_{-i,l})(x_i - x_i^*)$ , where  $x_i^* = \min_{x_s \in [x_{i,l}, x_{i,u}]} \int_{x_{i,l}}^{x_{i,u}} [f_j(x_i, x_{-i,l}) - f_j(x_s, x_{-i,l}) + f'_j(x_s, x_{-i,l})(x_i - x_s)] dx_s$ . A similar result obtains for where  $f_j(x)$  is concave over  $x_i$ . We can now use these single-dimensional bounds to obtain tighter lower and upper bounds on  $f_j(x)$  as follows. Note that for any  $c^l, c^u$  with  $\sum_i c_i^l = 1$  and  $\sum_i c_i^u = 1$ ,  $\sum_i c_i^l f_{j,i,lb}(x) \leq f_j(x) \leq \sum_i c_i^u f_{j,i,ub}(x)$ . Further, we can optimize  $c^l, c^u$  to obtain tight bounds. In practice, we can typically partition  $\mathcal{R}(\gamma)$  so that the stronger monotonicity and convexity or concavity assumptions hold for each  $\mathcal{R}_k$ .

Note that our linear bounds  $f_{lb}(x)$  and  $f_{ub}(x)$  introduce errors compared to the original nonlinear dynamics  $f$ . However, we can obtain tighter bounds by splitting  $\mathcal{R}_k$  further into subregions, and computing tighter bounds in each of the resulting subregions, but at the cost of increased computation. To balance these considerations, we only split a region  $\mathcal{R}_k$  if we obtain a counterexample in  $\mathcal{R}_k$  that is not an actual counterexample for the true dynamics  $f$ .

**Computing Bounds on ReLU Linearization Constants** In linearizing the ReLU activations, we supposed an existence of lower and upper bounds  $L$  and  $U$ . However, we cannot simply set  $L$  and  $U$  to some large negative and positive number, respectively, because  $V_\theta(x)$  has no a priori fixed bounds (in particular, note that for any Lyapunov function  $V$  and a constant  $a > 1$ ,  $aV$  is also a Lyapunov function). Thus, arbitrarily setting  $L$  and  $U$  makes verification unsound. To address this issue, we use interval bound propagation (IBP) (Gowal et al., 2018) to obtain an upper bound  $M = \max_{1 \leq i \leq n} \{|U_i|, |L_i|\}$ , where  $U_i$  is the upper bound, and  $L_i$  is the lower bound returned by IBP for the  $i$ -th layer, and the input to IBP are the upper and lower bounds of  $f(\mathcal{R}(\gamma))$ . Setting each  $L = -M$  and  $U = M$  then yields sound verification.

**Certifying Set Level and Computing ROA** The approaches above are instrumental in computing  $V_\theta$  and verifying the Lyapunov conditions over  $\mathcal{R}(\gamma)$ . The final piece is to connect this to computing a (subset of) ROA, which is our ultimate goal. To this end, let  $\mathcal{D}(\gamma, \rho) = \{x \in \mathcal{R}(\gamma) | V_\theta(x) < \rho\}$  be the sub-level set for  $\rho > 0$ . Now, recall that our verification is used to ensure that  $V_\theta$  and  $\pi_\beta$  satisfy  $V_\theta(f(x, \pi_\beta(x))) - V_\theta(x) < -\zeta$  for all  $x \in \mathcal{R}(\gamma)$  for a fixed  $\zeta > 0$ . We can then use this to prove that  $\mathcal{D}(\gamma, \rho)$  is a subset of the full ROA if for any  $x \in \mathcal{D}(\gamma, \rho)$ ,  $f(x, \pi_\beta(x)) \in \mathcal{D}(\gamma, \rho)$ .

**Lemma 3.1.** *Let  $\mathcal{D}(\gamma, \rho) = \{x \in \mathcal{R}(\gamma) | V_\theta(x) < \rho\}$ . Suppose  $x, f(x, \pi_\beta(x)) \in \mathcal{D}(\gamma, \rho)$  and  $V_\theta(f(x, \pi_\beta(x))) - V_\theta(x) < \zeta$  for all  $x \in \mathcal{R}(\gamma)$ , then  $\mathcal{D}(\gamma, \rho)$  is a subset of the ROA.*

*Proof Sketch.* This follows by simply noting that because time is discrete, starting from any  $x \in \mathcal{D}(\gamma, \rho)$ , we must be able to reach 0 within  $V_\theta(x)/\zeta$  time steps.  $\square$

Suppose that we are given an upper bound  $B(\gamma) \geq \sup_x \|f(x, \pi_\beta(x))\|_\infty$ . We can find  $\rho$ , and thereby obtain  $\mathcal{D}(\gamma, \rho)$ , by solving the following problem:

$$\min_{x \neq 0} z_K \tag{5a}$$

$$\text{s.t. : } \|x\|_\infty \leq \gamma \tag{5b}$$

$$\gamma \leq \|y\|_\infty \leq B(\gamma) \tag{5c}$$

$$z_{l+1} = g_{\theta_l}(z_l), \quad 0 \leq l \leq K-1 \tag{5d}$$

$$z_0 = y, \quad y \in \mathcal{X}. \tag{5e}$$

Note that we can transform problem (5) into a MILP by linearizing the ReLU activations as described above. We can then define  $\rho = z_K^*$ .

**Theorem 3.2.** *Given solution  $z_K^*$  to problem (5) and  $\rho = z_K^*$ ,  $\mathcal{D}(\gamma, \rho)$  is a subset of the ROA.*

*Proof.* For all  $x \in \mathcal{D}(\gamma, \rho)$ , since  $x \in \mathcal{R}(\gamma)$ , according to the Lyapunov property, we have  $V(f(x, u)) < V(x) < \rho$ . Since  $\rho = z_K^*$ , meaning  $f(x, u) \notin \mathcal{R}(B(\gamma)) \setminus \mathcal{R}(\gamma)$ ,  $f(x, u) \in \mathcal{R}(\gamma)$ . Thus,  $f(x, u) \in \mathcal{D}(\gamma, \rho)$ , and by Lemma 3.1,  $\mathcal{D}(\gamma, \rho)$  is a subset of ROA.  $\square$

## 4. Learning the Lyapunov Function and Policy

We cast learning the Lyapunov function and policy as the following problem:

$$\min_{\theta, \beta} \sum_{i \in S} \mathcal{L}(x_i; V_\theta, \pi_\beta), \quad (6)$$

where  $\mathcal{L}(\cdot)$  is a loss function that promotes Lyapunov learning and the set  $S \subseteq \mathcal{R}(\gamma)$  is a finite subset of points in the valid region. We assume that the loss function is differentiable, and consequently training follows a sequence of gradient update steps  $(\theta', \beta') = (\theta, \beta) - \mu \sum_{i \in S} \nabla_{\theta, \beta} \mathcal{L}(x_i; V_\theta, \pi_\beta)$ .

Clearly, the choice of the set  $S$  is pivotal to successfully learning  $V_\theta$  and  $\pi_\beta$  with provable stability properties. Prior approaches for learning Lyapunov functions represented by neural networks use one of two ways to generate  $S$ . The first is to generate a fixed set  $S$  comprised of uniformly random samples from the domain (Chang & Gao, 2021; Richards et al., 2018). However, this fails to learn verifiable Lyapunov functions. In the second,  $S$  is not fixed, but changes in each learning iteration, starting with randomly generated samples in the domain, and then using the verification tool, such as dReal, in each step of the learning process to update  $S$  (Chang et al., 2019; Zhou et al., 2022). However, verification is often slow, and becomes a significant bottleneck in the learning process.

Our key idea is to combine the benefits of these two ideas with a fast gradient-based heuristic approach for generating counterexamples. In particular, our proposed approach for training Lyapunov control functions and associated control policies (Algorithm 1; DITL) involves five parts:

1. an approach for heuristic counterexample generation (lines 10-12 of Algorithm 1),
2. an approach for choosing a collection  $S$  of inputs to update  $\theta$  and  $\beta$  in each training (gradient update) iteration (lines 9-13 of Algorithm 1),
3. the design of the loss function  $\mathcal{L}$ ,
4. initialization of policy  $\pi_\beta$  (line 3 of Algorithm 1), and
5. warm starting the training (line 4 of Algorithm 1).

We describe each of these next.

**Heuristic Counterexample Generation** As discussed in Section 3, verification in general involves two optimization problems:  $\min_{x \in \mathcal{R}(\gamma)} V_\theta(x) - V_\theta(f(x, \pi_\beta(x)))$  and  $\min_{x \in \mathcal{R}(\gamma)} V_\theta(x)$ . We propose a *projected gradient descent* (PGD) approach for approximating solutions to either of these problems. PGD proceeds as follows, using the second minimization problem as an illustration; the process is identical in the first case. Beginning with a starting point  $x_0 \in \mathcal{R}(\gamma)$ , we iteratively update  $x_{k+1}$ :

$$x_{k+1} = \Pi\{x_k + \alpha_k \text{sgn}(\nabla V_\theta(x_k))\},$$

where  $\Pi\{\cdot\}$  projects the gradient update step onto the domain  $\mathcal{R}(\gamma)$  by clipping each dimension of  $x_k$ , and  $\alpha_k$  is the PGD learning rate. Note that as  $f$  is typically differentiable, we can take gradients directly through it when we apply PGD for the first verification problem above.

We run this procedure for  $K$  iterations, and return the result (which may or may not be an actual counterexample). Let  $T' = \text{PGD}(T)$  denote running PGD for a set of  $T$  starting points for both of the optimization problems above, resulting in a corresponding set  $T'$  of possible counterexamples.

**Selecting Inputs for Gradient Updates** A natural idea for selecting samples  $S$  is to simply add counterexamples identified in each iteration of the Lyapunov learning process. However, as  $S$  then grows without bound, this progressively slows down the learning process. In addition, it is important for  $S$  to contain a relatively broad sample of the valid region to ensure that counterexamples we generate along the way do not cause undesired distortion of  $V_\theta$  and  $\pi_\beta$  in subregions not

---

**Algorithm 1** DITL Lyapunov learning algorithm.
 

---

```

1: Input: Dynamical system model  $f(x, u)$  and target valid region  $\mathcal{R}(\gamma)$ 
2: Output: Lyapunov function  $V_\theta$  and control policy  $\pi_\beta$ 
3:  $\pi_\beta = \text{Initialize}()$ 
4:  $V_\theta = \text{PreTrainLyapunov}(N_0, \pi_\beta)$ 
5:  $B = \text{InitializeBuffer}()$ 
6:  $W \leftarrow \emptyset$ 
7: while True do
8:   for  $N$  iterations do
9:      $\hat{S} = \text{Sample}(r, B)$  //sample  $r$  points from  $B$ 
10:     $T = \text{Sample}(q, \mathcal{R}(\gamma))$  //sample  $q$  points from  $\mathcal{R}(\gamma)$ 
11:     $T' = \text{PGD}(T)$ 
12:     $T'' = \text{FilterCounterExamples}(T')$ 
13:     $S = \hat{S} \cup T'' \cup W$ 
14:     $B = B \cup T''$ 
15:     $(\theta, \beta) \leftarrow (\theta, \beta) - \mu \sum_{i \in S} \nabla_{\theta, \beta} \mathcal{L}(x_i; V_\theta, \pi_\beta)$ 
16:  end for
17:  (success,  $\hat{W}$ ) =  $\text{Verify}(V_\theta, \pi_\beta)$ 
18:  if success then
19:    return  $V_\theta, \pi_\beta$ 
20:  else
21:     $W \leftarrow W \cup \hat{W}$ 
22:  end if
23: end while
24: return FAILED // Timeout
    
```

---

well represented in  $S$ . Finally, we need to retain the memory of previously generated counterexamples, as these are often particularly challenging parts of the input domain for learning. We therefore construct  $S$  as follows.

We create an input buffer  $B$ , and initialize it with a random sample of inputs from  $\mathcal{R}(\gamma)$ . Let  $W$  denote a set of counterexamples generated that we wish to remember through the entire training process, initialized to be empty. In our implementation,  $W$  consists of all counterexamples generated by the sound verification tools described in Section 3.

At the beginning of each training update iteration, we randomly sample a fixed-size subset  $\hat{S}$  of the buffer  $B$ . Next, we take a collection  $T$  of random samples from  $\mathcal{R}$  to initialize PGD, and generate  $T' = \text{PGD}(T)$ . We then filter out all the counterexamples from  $T'$ , retaining only those with either  $V_\theta(x) \leq 0$  or  $V_\theta(x) - V_\theta(f(x, \pi_\beta(x))) \leq \epsilon$ , where  $\epsilon$  is a non-negative hyperparameter; this yields a set  $T''$ . We then use  $S = \hat{S} \cup T'' \cup W$  for the gradient update in the current iteration. Finally, we update the buffer  $B$  by adding to it  $T''$ . This process is repeated for  $N$  iterations.

After  $N$  iterations, we check to see if we have successfully learned a stable policy and a Lyapunov control function by using the tools from Section 3 to verify  $V_\theta$  and  $\pi_\beta$ . If verification succeeds, training is complete. Otherwise, we use the counterexamples  $\hat{W}$  generated by the MILP solver to update  $W = W \cup \hat{W}$ , and repeat the learning process above.

**Loss Function Design** Next, we design of the loss function  $\mathcal{L}(x; V_\theta, \pi_\beta)$  for a given input  $x$ . A key ingredient in this loss function is a term that incentivizes the learning process to satisfy Lyapunov condition (2c):  $\mathcal{L}_1(x; V_\theta, \pi_\beta) = \text{ReLU}(V_\theta(f(x, \pi_\beta(x))) - V_\theta(x) + \eta)$ , where the parameter  $\eta \geq 0$  determines how aggressively we try to satisfy this condition during learning.

In order to learn a Lyapunov function satisfying Condition (2a) and (2b), we have several options. The simplest option is to set all bias terms in the neural network to zero ( $b_j = 0$  for all linear units  $j$ ). Doing so immediately satisfies  $V_\theta(0) = 0$ . An effective way to deal with Condition (2b) is to maximize the lower bound on  $V_\theta(x)$ . To this end, we propose to make use of the following loss term:  $\mathcal{L}_2(x; V_\theta, \pi_\beta) = \text{ReLU}(-V_\theta^{LB})$ , where  $V_\theta^{LB}$  is the lower bound on the Lyapunov function over the target domain  $\mathcal{R}(\gamma)$ . We can obtain this lower bound using any differentiable neural network certification technique; in particular, we use  $\alpha, \beta$ -CROWN (Zhang et al., 2022) for this purpose.

The downside of setting bias terms to zero is that we lose many learnable parameters, reducing flexibility of the neural

network. If we consider a general neural network, on the other hand, it is no longer the case that  $V_\theta(x) = 0$  by construction. However, it is straightforward to ensure this by defining the final Lyapunov function as  $\tilde{V}_\theta(x) = V_\theta(x) - V_\theta(0)$ . Now, satisfying Condition (2b) amounts to satisfying the condition that  $V_\theta(x) \geq V_\theta(0)$ , which we accomplish via the following pair of loss terms:  $\mathcal{L}_3(x; V_\theta, \pi_\beta) = \text{ReLU}(V_\theta(0) - V_\theta(x) + \mu \min(\|x\|_2, \nu))$ , where  $\mu$  and  $\nu$  are hyperparameters of the term  $\mu \min(\|x\|_2, \nu)$  which effectively penalizes  $V_\theta(x)$  for being too large, and  $\mathcal{L}_4(x; V_\theta, \pi_\beta) = \|V_\theta(0)\|_2^2$ .

The general loss function is then a weighted sum of these loss terms,

$$\mathcal{L}(x; V_\theta, \pi_\beta) = \mathcal{L}_1(x; V_\theta, \pi_\beta) + c_2 \mathcal{L}_2(x; V_\theta, \pi_\beta) + c_3 \mathcal{L}_3(x; V_\theta, \pi_\beta) + c_4 \mathcal{L}_4(x; V_\theta, \pi_\beta).$$

When we set bias terms to zero, we would set  $c_3 = c_4 = 0$ ; otherwise, we set  $c_2 = 0$ .

**Initialization** We consider two approaches for initializing the policy  $\pi_\beta$  ( $V_\theta$  is initialized randomly). The first is to linearize the dynamics  $f$  around the origin, and use a policy computing based on a linear quadratic regulator (LQR) to obtain a simple linear policy  $\pi_\beta$ . The second approach is to use deep reinforcement, such as PPO (Liu et al., 2019), where rewards correspond to stability (e.g., reward is the negative value of the  $l_2$  distance of state to origin). We view the choice between these as a hyperparameter in our approach. To initialize  $V_\theta$ , we fix  $\pi_\beta$  after its initialization, and follow our learning procedure above using solely heuristic counterexample generation to pre-train  $V_\theta$ .

The next result now follows by construction.

**Theorem 4.1.** *If Algorithm 1 returns  $V_\theta, \pi_\beta$ , they are guaranteed to satisfy conditions (2).*

## 5. Experiments

### 5.1. Experiment Setup

**Benchmark Domains** Our evaluation of the proposed DITL approach uses four benchmark control domains: *inverted pendulum*, *path tracking*, *cartpole*, and *drone planar vertical takeoff and landing (PVTOL)*. Since these are described as continuous-time domains, we set the time between state updates to be  $0.05s$  in all cases for our discretized versions of these systems. Details about these domains, including the dynamical system models, are provided in the Appendix.

**Baselines** We compare the proposed approach to four baselines: *linear quadratic regulator (LQR)*, *sum-of-squares (SOS)*, *neural Lyapunov control (NLC)* (Chang et al., 2019), and *neural Lyapunov control for unknown systems (UNL)* (Zhou et al., 2022). The first two, LQR and SOS, are the more traditional approaches for computing Lyapunov functions when the dynamics are either linear (LQR) or polynomial (SOS) (Tedrake, 2009). LQR solutions (when the system can be stabilized) are obtained through matrix multiplication, while SOS entails solving a semidefinite program (we solve it using YALMIP with MOSEK solver in MATLAB 2022b). The next two baselines, NLC and UNL, are recent approaches for learning Lyapunov functions in continuous-time systems (no approach for learning provably stable control using neural network representations exists for discrete time systems). Both NLC and UNL yield provably stable control for general non-linear dynamical systems, and are thus the most competitive baselines to date. In addition to these baselines, we consider an ablation in which PGD-based counterexample generation for our approach is entirely replaced by the sound MILP-based method during learning (we refer to it as DITL-MILP).

**Efficacy Metrics** We compare approaches in terms of three efficacy metrics. The first is (serial) runtime (that is, if no parallelism is used), which we measure as wall clock time when only a single task is running on a machine. For inverted pendulum and path tracking, all comparisons were performed on a machine with AMD Ryzen 9 5900X 12-Core Processor and Linux Ubuntu 20.04.5 LTS OS. All cartpole and PVTOL experiments were run on a machine with a Xeon Gold 6150 CPU (64-bit 18-core x86), Rocky Linux 8.6. UNL and RL training for Path Tracking are the only two cases that make use of GPUs, and was run on NVIDIA GeForce RTX 3090.

The second metric was the size of the valid region, measured using  $l_2$  norm for NLC and UNL, and  $l_\infty$  norm (which dominates  $l_2$ ) for LQR, SOS, and our approach. We exclude a region  $\|x\|_\infty < 0.1$  to ensure numerical stability for all  $l_\infty$  approaches, and use a larger region for all  $l_2$  baselines. The third metric is the *region of attraction (ROA)*. Whenever verification fails, we set ROA to 0. Finally, we compare all methods whose results are stochastic (NLC, UNL, and ours) in terms of *success rate*.

**Verification Details** For LQR, SOS, NLC, and UNL, we used dReal as the verification tool, as done by Chang et al. (2019) and Zhou et al. (2022). We used CPLEX version 22.1.0 for verification.

Table 1. Inverted Pendulum

	Valid Region	Runtime (s)	ROA	Max ROA	Success Rate
NLC (free)	$\ x\ _2 \leq 6.0$	$28 \pm 29$	$11 \pm 4.6$	22	100%
NLC (max torque 6.0)	$\ x\ _2 \leq 6.0$	$519 \pm 184$	$13 \pm 27$	66	20%
UNL (max torque 6.0)	$\ x\ _2 \leq 4.0$	$821 \pm 227$	$1 \pm 2$	7	30%
LQR	$\ x\ _\infty \leq 5.8$	< <b>1</b>	14	14	success
SOS	$\ x\ _\infty \leq 1.7$	< <b>1</b>	6	6	success
DITL	$\ x\ _\infty \leq 12$	$8.1 \pm 4.7$	<b>61 ± 31</b>	<b>123</b>	100%

### 5.2. Results

**Inverted Pendulum** For the inverted pendulum domain, we initialize the control policy using the LQR solution (see Appendix for details). Consequently, we consider a linear policy  $\pi_\beta$ . We train a ReLU network for  $V_\theta$  with non-zero bias terms. We consider NLC both with and without an upper bound on force; an upper bound is 6N where relevant. We approximate ROA using a grid of 2000 cells along each coordinate using the level set certified with MILP (5). All runtime is capped at 600 seconds, except the UNL baseline, which we cap at 16 minutes, as it tends to be considerably slower than other methods.

Our results are presented in Table 1. While LQR and SOS yield the fastest runtime, our approach (DITL) is the next fastest, taking on average  $\sim 8$  seconds, with NLC and UNL considerably slower. However, DITL yields an ROA *a factor >4 larger* than the nearest baseline (LQR), and 100% success rate. In contrast, the corresponding NLC variant with maximum force has only a 20% success rate, while the more successful NLC approach without force constraint yields smaller ROA. Finally, we find that the DITL-MILP ablation is two orders of magnitude slower (runtime > 300 seconds) *and* less effective (average ROA=42, 80% success rate) than DITL, demonstrating the significance of using heuristic counterexample generation during training. We visualize comparison of maximum ROA produced by all methods in Figure 1 (left).

Table 2. Path Tracking

	Valid Region	Runtime (s)	ROA	Max ROA	Success Rate
NLC	$\ x\ _2 \leq 1.0$	$109 \pm 81$	$0.5 \pm 0.2$	0.76	100%
NLC	$\ x\ _2 \leq 1.5$	$151 \pm 238$	$1.4 \pm 0.9$	2.8	80%
UNL	$\ x\ _2 \leq 0.8$	$925 \pm 110$	$0.1 \pm 0.2$	0.56	10%
LQR	$\ x\ _\infty \leq 0.7$	< <b>1</b>	1.02	1.02	success
SOS	$\ x\ _\infty \leq 0.8$	< <b>1</b>	1.8	1.8	success
DITL (LQR)	$\ x\ _\infty \leq 3.0$	$9.8 \pm 4$	$8 \pm 3$	12.5	100%
DITL (RL)	$\ x\ _\infty \leq 3.0$	$14 \pm 11$	<b>9 ± 3.5</b>	<b>16</b>	100%

**Path Tracking** In path tracking, we initialize our approach using both the RL and LQR solutions, drawing a direct comparison between the two. For RL, the reward function is  $-\frac{1}{10}(e_{ra}^2 + \theta_e^2)^{1/2}$ , and we use PPO (Schulman et al., 2017), training over 50K steps (see Appendix for further details). The running time of RL is 154.96 seconds.

The results are provided in Table 2. We can observe that both RL- and LQR-initialized variants of our approach outperform all prior art, with RL exhibiting *a factor of 5 advantage* over the next best (SOS, in this case) in terms of ROA, and nearly a factor of 6 advantage in terms of maximum achieved ROA (NLC is the next best in this case). Moreover, our approach again has a 100% success rate. Our runtime is an order of magnitude lower than NLC or UNL, but both LQR and SOS are subsecond in this case, considerably better than ours, which clocks in at approximately 10-15 seconds on average. Overall, the RL-initialized variant outperforms LQR initialization, albeit only slightly in terms of average ROA, though more substantively in terms of maximum achieved ROA. The DITL-MILP ablation again performs far worse than DITL: running time is several orders of magnitude slower (at > 550 seconds), with low efficacy (ROA is 1.1, success rate 10%). We visualize comparison of maximum ROA produced by all methods in Figure 1 (right).

**Cartpole** For the cartpole domain, we used LQR for initialization, and set bias terms of  $V_\theta$  to zero, simplifying the learning problem. We set the running time limit to 2 hours for all approaches. None of the baselines successfully attained a



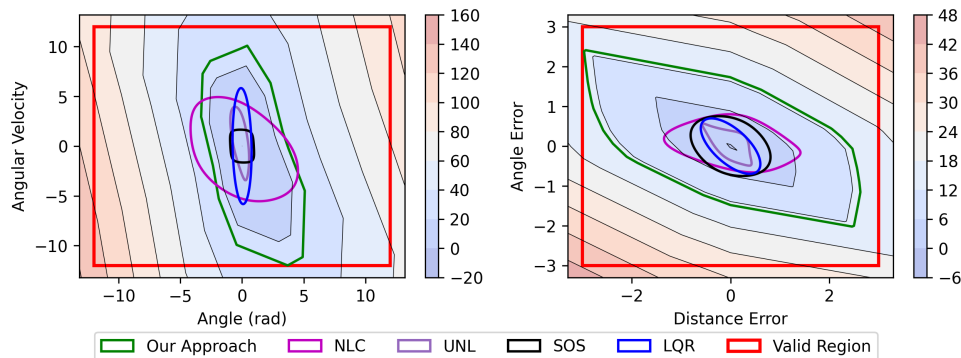


Figure 1. ROA plot of inverted pendulum (left) and path tracking (right). We select the best result for each method.

provably stable control policy and associated Lyapunov function for this problem. Failure was either because we could find counterexamples within the target valid region, or because the verification process itself took longer than the time limit. In contrast, the proposed DITL approach found a valid region of  $\|x\|_\infty \leq 1.0$ , taking no more than 1.6 hours total, and 0.85 hours on average, yielding a 100% success rate. The ROA we found was  $0.021 \pm 0.012$ . To provide a sense of what this ROA means, we projected the region onto each state variable, obtaining ranges:  $x \in [-0.8, 0.8]$ ,  $\dot{x} \in [-0.9, 1]$ ,  $\theta \in [-0.1, 0.1]$ , and  $\dot{\theta} \in [-0.3, 0.3]$ .

**PVTOL** For PVTOL, the setup was similar to the cartpole domain. We set bias terms of  $V_\theta$  to zero, simplifying the learning problem. We set the maximum running time at 24 hours. None of the baselines successfully identified a provably stable control policy and Lyapunov function within 24 hours. In contrast, our approach found one within  $13 \pm 6$  hours on average, yielding a 100% success rate. We identified a valid region of  $\|x\|_\infty \leq 1.0$ , and obtained ROA of  $0.011 \pm 0.008$  and maximum ROA of 0.028. Projecting this ROA on each dimension of this problem, we obtain the following variable ranges:  $x, y \in [-1, 1]$ ,  $\dot{x} \in [-0.6, 0.6]$ ,  $\dot{y} \in [-0.5, 0.4]$ ,  $\theta \in [-0.1, 0.1]$ , and  $\dot{\theta} \in [-0.9, 1]$ .

## 6. Conclusion

We presented a novel algorithmic framework for learning Lyapunov control functions and associated stabilizing control policies for discrete-time nonlinear dynamical systems. Our approach combines mixed-integer linear programming verification tool with a training procedure that leverages gradient-based approximate verification. This combination enables a significant improvement in effectiveness compared to prior art: our experiments demonstrate that our approach yields several factors larger regions of attraction in two simpler benchmark domains (inverted pendulum and path tracking), and ours is the only approach that successfully finds stable policies on two more challenging benchmarks (cartpole and PVTOL).

## References

- Abate, A., Ahmed, D., Giacobbe, M., and Peruffo, A. Formal synthesis of lyapunov neural networks. *IEEE Control Systems Letters*, 5(3):773–778, 2020.
- Berkenkamp, F., Turchetta, M., Schoellig, A., and Krause, A. Safe model-based reinforcement learning with stability guarantees. *Advances in neural information processing systems*, 30, 2017.
- Bertsimas, D. and Tsitsiklis, J. N. *Introduction to linear optimization*, volume 6. Athena scientific Belmont, MA, 1997.
- Chang, Y.-C. and Gao, S. Stabilizing neural control using self-learned almost lyapunov critics. In *IEEE International Conference on Robotics and Automation*, pp. 1803–1809, 2021.
- Chang, Y.-C., Roohi, N., and Gao, S. Neural lyapunov control. In *Neural Information Processing Systems*, 2019.
- Chen, S., Fazlyab, M., Morari, M., Pappas, G. J., and Preciado, V. M. Learning lyapunov functions for hybrid systems. In *Proceedings of the 24th International Conference on Hybrid Systems: Computation and Control*, pp. 1–11, 2021a.

- Chen, S., Fazlyab, M., Morari, M., Pappas, G. J., and Preciado, V. M. Learning region of attraction for nonlinear systems. In *2021 60th IEEE Conference on Decision and Control (CDC)*, pp. 6477–6484. IEEE, 2021b.
- Choi, J., Castaneda, F., Tomlin, C. J., and Sreenath, K. Reinforcement learning for safety-critical control under model uncertainty, using control lyapunov functions and control barrier functions. *arXiv preprint arXiv:2004.07584*, 2020.
- Dai, H., Landry, B., Yang, L., Pavone, M., and Tedrake, R. Lyapunov-stable neural-network control. In *Robotics: Science and Systems (RSS)*, 2021.
- Donti, P. L., Roderick, M., Fazlyab, M., and Kolter, J. Z. Enforcing robust control guarantees within neural network policies. In *International Conference on Learning Representations*, 2021.
- Gao, S., Kong, S., and Clarke, E. M. dreal: An smt solver for nonlinear theories over the reals. In *International conference on automated deduction*, pp. 208–214. Springer, 2013.
- Gowal, S., Dvijotham, K., Stanforth, R., Bunel, R., Qin, C., Uesato, J., Arandjelovic, R., Mann, T., and Kohli, P. On the effectiveness of interval bound propagation for training verifiably robust models. *arXiv preprint arXiv:1810.12715*, 2018.
- Han, M., Zhang, L., Wang, J., and Pan, W. Actor-critic reinforcement learning for control with stability guarantee. *IEEE Robotics and Automation Letters*, 5(4):6217–6224, 2020.
- Khalil, H. K. *Nonlinear control*, volume 406. Pearson New York, 2015.
- Kolter, J. Z. and Manek, G. Learning stable deep dynamics models. *Advances in neural information processing systems*, 32, 2019.
- Liu, B., Cai, Q., Yang, Z., and Wang, Z. Neural trust region/proximal policy optimization attains globally optimal policy. In *neural information processing systems*, 2019.
- Raffin, A. RL baselines3 zoo. <https://github.com/DLR-RM/rl-baselines3-zoo>, 2020.
- Ravanbakhsh, H. and Sankaranarayanan, S. Learning control lyapunov functions from counterexamples and demonstrations. *Autonomous Robots*, 43(2):275–307, 2019.
- Rego, R. C. and de Araújo, F. M. Learning-based robust neuro-control: A method to compute control lyapunov functions. *International Journal of Robust and Nonlinear Control*, 32(5):2644–2661, 2022.
- Richards, S. M., Berkenkamp, F., and Krause, A. The lyapunov neural network: Adaptive stability certification for safe learning of dynamical systems. In *Conference on Robot Learning*, pp. 466–476. PMLR, 2018.
- Schulman, J., Wolski, F., Dhariwal, P., Radford, A., and Klimov, O. Proximal policy optimization algorithms. *arXiv preprint arXiv:1707.06347*, 2017.
- Singh, S., Richards, S. M., Sindhvani, V., Slotine, J.-J. E., and Pavone, M. Learning stabilizable nonlinear dynamics with contraction-based regularization. *The International Journal of Robotics Research*, 40(10-11):1123–1150, 2021.
- Snider, J. M. Automatic steering methods for autonomous automobile path tracking. *Robotics Institute, Pittsburgh, PA, Tech. Rep. CMU-RITR-09-08*, 2009.
- Tedrake, R. Underactuated robotics: Learning, planning, and control for efficient and agile machines course notes for mit 6.832. *Working draft edition*, 3:4, 2009.
- Zhang, H., Wang, S., Xu, K., Li, L., Li, B., Jana, S., Hsieh, C.-J., and Kolter, J. Z. General cutting planes for bound-propagation-based neural network verification. In *Advances in Neural Information Processing Systems*, 2022.
- Zhou, R., Quartz, T., De Sterck, H., and Liu, J. Neural lyapunov control of unknown nonlinear systems with stability guarantees. In *Neural Information Processing Systems*, 2022.

## A. Further Details about Experiments

### A.1. Dynamics

**Inverted Pendulum** We use the following standard dynamics model for inverted pendulum (Chang et al., 2019; Richards et al., 2018; Zhou et al., 2022):

$$\ddot{\theta} = \frac{mg\ell \sin(\theta) + u - b\dot{\theta}}{m\ell^2},$$

with gravity constant  $g = 9.81$ , ball weight  $m = 0.15$ , friction  $b = 0.1$ , and pendulum length  $l = 0.5$ . We set the maximum force allowed to be  $6N$ , meaning  $u \in [-6.0, 6.0]$ , and it is applied to all experiments except for the NLC (free) case.

**Path Tracking** Our *path tracking* dynamics follows Snider (2009) and Chang et al. (2019):

$$\begin{aligned} \dot{s} &= \frac{v \cos(\theta_e)}{1 - \dot{e}_{ra}\kappa(s)}, \quad \dot{e}_{ra} = v \sin(\theta_e), \\ \dot{\theta}_e &= \frac{v \tan(\delta)}{L} - \frac{v\kappa(s) \cos(\theta_e)}{1 - \dot{e}_{ra}\kappa(s)}, \end{aligned}$$

where the control policy determines the steering angle  $\delta$ .  $e_{ra}$  is the distance error and  $\theta_e$  is the angle error. We can simplify the dynamics by defining  $u = \tan(\delta)$ , so that non-linearity of dynamics is only in terms of state variables. Since in practice  $|\delta| \leq 40^\circ$ , we set  $u \in [\tan(-40^\circ), \tan(40^\circ)]$ ; this is applied to all experiments. We set speed  $v = 2.0$ , while the track is a circle with radius 10.0 (and, thus,  $\kappa = 0.1$ ) and  $L = 1.0$ .

**Cartpole** For *cartpole* we use the following dynamics from Tedrake (2009). The original dynamics is

$$\ddot{x} = \frac{1}{m_c + m_p \sin^2 \theta} \left[ f_x + m_p \sin \theta (l\dot{\theta}^2 + g \cos \theta) \right] \quad (7)$$

$$\ddot{\theta} = \frac{1}{l(m_c + m_p \sin^2 \theta)} \left[ -f_x \cos \theta - m_p l \dot{\theta}^2 \cos \theta \sin \theta - (m_c + m_p)g \sin \theta \right]. \quad (8)$$

We change the variable and rename  $\pi - \theta$  as  $\theta$ , so that in our setting,  $\theta$  represents the angle between the pole and the upward horizontal direction, the pole angle is positive if it is to the right. The purpose of this transformation is that the equilibrium point is the origin.

Using the second order chain rule

$$\frac{d^2y}{dz^2} = \frac{d^2y}{du^2} \left( \frac{du}{dz} \right)^2 + \frac{dy}{du} \frac{d^2u}{dz^2}$$

let  $y = \pi - \theta$ ,  $z = t$ ,  $u = \theta$ , we have the new dynamics as

$$\ddot{x} = \frac{1}{m_c + m_p \sin^2 \theta} \left[ f_x + m_p \sin \theta (l\dot{\theta}^2 - g \cos \theta) \right] \quad (9)$$

$$\ddot{\theta} = \frac{1}{l(m_c + m_p \sin^2 \theta)} \left[ -f_x \cos \theta - m_p l \dot{\theta}^2 \cos \theta \sin \theta + (m_c + m_p)g \sin \theta \right]. \quad (10)$$

Here  $m_c = 1.0$  is the weight of the cart,  $m_p = 0.1$  is the weight of the pole,  $x$  is the horizontal position of the cart,  $l = 1.0$  is the length of the pole,  $g = 9.81$  is the gravity constant and  $f_x$  is the controller (force applied to the cart). Furthermore, the maximum force allowed to the cart is set to be  $30N$ , meaning  $f_x \in [-30, 30]$ ; this is applied to all experiments.

**PVTOL** For *PVTOL*, our dynamics follows Singh et al. (2021). Specifically, the system has the following state representation:  $x = (p_x, p_z, v_x, v_z, \phi, \dot{\phi})$ .  $(p_x, p_z)$  and  $(v_x, v_z)$  are the 2D position and velocity, respectively, and  $(\phi, \dot{\phi})$  are the roll

and angular rate. Control  $u \in \mathbb{R}_{>0}^2$  corresponds to the controlled motor thrusts. The dynamics  $f(x, u)$  are described by

$$\dot{x}(t) = \begin{bmatrix} v_x \cos \phi - v_z \sin \phi \\ v_x \sin \phi + v_z \cos \phi \\ \dot{\phi} \\ v_z \dot{\phi} - g \sin \phi \\ -v_x \dot{\phi} - g \cos \phi \\ 0 \end{bmatrix} + \begin{bmatrix} 0 & 0 \\ 0 & 0 \\ 0 & 0 \\ 0 & 0 \\ (1/m) & (1/m) \\ l/J & (-l/J) \end{bmatrix} u$$

where  $g = 9.8$  is the acceleration due to gravity,  $m = 4.0$  is the mass,  $l = 0.25$  is the moment-arm of the thrusters, and  $J = 0.0475$  is the moment of inertia about the roll axis. The maximum force allowed to both  $u_1$  and  $u_2$  is set to be  $39.2N$ , which is  $mg$ , meaning  $u_1, u_2 \in [0, 39.2]$ ; this is applied to all experiments.

## A.2. Computation of the LQR Solution

Given the system  $dx/dt = Ax + Bu$ , the objective function of the LQR is to compute the optimal controller  $u = -Kx$  that minimizes the quadratic cost  $\int_0^\infty (x'Qx + u'Ru)dt$ , where  $R$  and  $Q$  are identity matrices. The details of the system linearization as well as the LQR solution are described below.

**Inverted Pendulum** We linearize the system as

$$A = \begin{bmatrix} 0 & 1 \\ g/l & -b/ml^2 \end{bmatrix}, B = \begin{bmatrix} 0 \\ 1/ml^2 \end{bmatrix}$$

The final LQR solution is  $u = -1.97725234\theta - 0.97624064\dot{\theta}$ .

**Path Tracking** We linearize the system as

$$A = \begin{bmatrix} 0 & 2 \\ 0 & -0.04 \end{bmatrix}, B = \begin{bmatrix} 0 \\ 1 \end{bmatrix}.$$

The final LQR solution is  $u' = 2u + 0.1 = -e_{ra} - 2.19642572\theta_e$ .

**Cartpole** We linearize the system as

$$A = \begin{bmatrix} 0 & 1 & 0 & 0 \\ 0 & 0 & -0.98 & 0 \\ 0 & 0 & 0 & 1 \\ 0 & 0 & 10.78 & 0 \end{bmatrix}, B = \begin{bmatrix} 0 \\ 1 \\ 0 \\ -1 \end{bmatrix}.$$

The final LQR solution is  $u = x + 2.4109461\dot{x} + 34.36203947\theta + 10.70094483\dot{\theta}$ .

**PVTOL** We linearize the system as

$$A = \begin{bmatrix} 0 & 0 & 0 & 1 & 0 & 0 \\ 0 & 0 & 0 & 0 & 1 & 0 \\ 0 & 0 & 0 & 0 & 0 & 1 \\ 0 & 0 & -g & 0 & 0 & 0 \\ 0 & 0 & 0 & 0 & 0 & 0 \\ 0 & 0 & 0 & 0 & 0 & 0 \end{bmatrix}, B = \begin{bmatrix} 0 & 0 \\ 0 & 0 \\ 0 & 0 \\ 0 & 0 \\ \frac{1}{m} & \frac{1}{m} \\ \frac{r}{J} & -\frac{r}{J} \end{bmatrix}$$

The final LQR solution is  $u_1 = 0.70710678x - 0.70710678y - 5.03954871\theta + 1.10781077\dot{x} - 1.82439774\dot{y} - 1.20727555\dot{\theta}$ , and  $u_2 = -0.70710678x - 0.70710678y + 5.03954871\theta - 1.10781077\dot{x} - 1.82439774\dot{y} + 1.20727555\dot{\theta}$ .

## A.3. PPO Training for Path Tracking

We use the implementation in Stable-Baselines (Raffin, 2020) for PPO training. The hyperparameters of are fine-tuned using their auto-tuning script with a budget of 1000 trials with a maximum of 50000 steps. The final hyperparameters are in Table 3.

Table 3. Hyperparameter for PPO (Path Tracking)

POLICY	MLPPOLICY
N_TIMESTEPS	!!FLOAT 100000
BATCH_SIZE	32
N_STEPS	64
GAMMA	0.95
LEARNING_RATE	0.000208815
ENT_COEF	1.90E-06
CLIP_RANGE	0.1
N_EPOCHS	10
GAE_LAMBDA	0.99
MAX_GRAD_NORM	0.8
VF_COEF	0.550970466
ACTIVATION_FN	NN.ReLU
LOG_STD_INIT	-0.338380542
ORTHO_INIT	FALSE
NET_ARCH	[8, 8]
VF	[8, 8]
SDE_SAMPLE_FREQ	128

#### A.4. Benchmark Models

When relevant, benchmark models (as well as our approach) are run for 10 seeds (seed 0 to 9). Mean  $\pm$  standard deviation are reported in Table 1 and Table 2. For SOS benchmark, we use polynomials of degree  $\leq 6$  for all environments.

**NLC and UNL** For Cartpole and PVTOL, we train against diameter 1.0 under the  $l_2$  norm for NLC and UNL. The main reason for the failure of training is that the dReal verifier becomes incredibly slow after some iterations. For example, for seed 0, NLC only finished 167 certifications within 2 hours limit for Cartpole, and 394 certifications within 24 hours limit for PVTOL.

**LQR and SOS** For Cartpole environment, we first certify against target region  $0.1 \leq \|x\|_\infty \leq 0.16$  for LQR benchmark where dReal returns the counterexample; we later attempt to certify against  $0.1 \leq \|x\|_\infty \leq 0.15$ , dReal did not return any result within the 2-hour limit. For SOS benchmark, dReal verifier did not return any result within the 2 hours limit against target region  $0.1 \leq \|x\|_\infty \leq 0.5$ . For PVTOL environment, LQR benchmark returns the counterexample against target region  $0.1 \leq \|x\|_\infty \leq 0.5$  after 10 hours, we then attempt to certify against  $0.1 \leq \|x\|_\infty \leq 0.4$  and fail to return any result within the remaining 14 hours time limit. For SOS benchmark, dReal verifier did not return any result within the 24 hours limit against target region  $0.1 \leq \|x\|_\infty \leq 0.5$ .

#### A.5. Bounding the Functions

There are three types of bounding in our paper: 1) bound the dynamics  $f(x, u)$  with linear upper/lower bound functions for verification; 2) bound the dynamics with constants for the calculation of  $M$  for ReLU; 3) bound the dynamics with constants for the calculation of ROA. Note that the bounding for 2) and 3) are similar, except that for 2) it is calculated for each subgrid, and for 3) it is calculated for the entire valid region.

**Inverted Pendulum** Split the region: we split the region over the domain of  $\theta$ , with intervals endpoints as [-12.0, -11.0, -10.0, -9.0, -8.0, -7.0, -6.0, -5.0, -4.0, -3.0, -2.0, -1.0, -0.5, -0.1], [0.1, 0.5, 1.0, 2.0, 3.0, 4.0, 5.0, 6.0, 7.0, 8.0, 9.0, 10.0, 11.0, 12.0] while the interval of  $\dot{\theta}$  is [-12, 12], as well as  $\theta \in [-1.0, 0.1]$ ,  $\dot{\theta} \in [0.1, 12]$ , and  $\theta \in [-1.0, 0.1]$ ,  $\ddot{\theta} \in [-12, -0.1]$ .

1) Bound for verification: since the only non-linear part of the function is  $\sin(\theta)$ , we use the upper/lower bounds in  $\alpha, \beta$ -CROWN.

2) Bound for  $M$ :  $|\dot{\theta}| \leq \frac{g}{l} + \frac{|u|_{\max}}{ml^2} + \frac{b|\dot{\theta}|_{\max}}{ml^2}$ , where  $|u|_{\max}$  is calculated using IBP bound.

3) Bound for ROA:  $\|f(x, u)\|_\infty = \gamma + \max(\gamma, \frac{mgl + |u|_{\max} + b\gamma}{ml^2})dt$ , where  $|u|_{\max}$  is the maximum force allowed.

**Path Tracking** Split the region: we split the region over the domain of  $\theta_e$ , with interval endpoints as  $[-3.0, -2.5, -2.0, -\pi/2, -1.0, -0.5, -0.1], [0.1, 0.5, 1.0, \pi/2, 2.0, 2.5, 3.0]$  while the interval of  $e_{ra}$  is  $[-3.0, 3.0]$ , as well as  $\theta_e \in [-0.1, 0.1], e_{ra} \in [0.1, 3.0]$ , and  $\theta_e \in [-0.1, 0.1], e_{ra} \in [-3.0, -0.1]$ .

- 1) Bound for verification: for  $\dot{e}_{ra}$  since the only nonlinear function is  $\sin(\theta)$ , we use the bound in  $\alpha, \beta$ -CROWN; for  $\dot{\theta}_e$  we bound the term  $\frac{v\kappa(s)\cos(\theta_e)}{1-\dot{e}_{ra}\kappa(s)}$ , which is concave in interval  $[-\pi/2, \pi/2]$ , and convex otherwise.
- 2) Bound for  $M$ :  $|\dot{e}_{ra}| \leq v, |\dot{\theta}_e| \leq \frac{v|u|_{\max}}{L} + \frac{v}{R-v}$ , where  $|u|_{\max}$  is calculated using IBP bound.
- 3) Bound for ROA:  $\|f(x, u)\|_{\infty} = \gamma + \max(v, \frac{v|u|_{\max}}{L} + \frac{v}{R-v})dt$ , where  $|u|_{\max}$  is the maximum force allowed.

**Cartpole** Split the region: we split the region over the domain of  $\theta$  and  $\dot{\theta}$  with interval 0.1 when either  $\theta$  or  $\dot{\theta}$  is greater than 0.1. In case when both  $\theta$  and  $\dot{\theta}$  are smaller than 0.1, we split  $\theta, \dot{\theta}$  into intervals of 0.05.

- 1) Bound for verification: we split the dynamics into six functions and bound them separately for both one variable and multiple variables:  $f_1 = \frac{1}{m_c+m_p \sin^2 \theta}, f_2 = \frac{-\cos \theta}{l(m_c+m_p \sin^2 \theta)}, f_3 = \frac{-gm_p \sin \theta \cos \theta}{m_c+m_p \sin^2 \theta}, f_4 = \frac{(m_c+m_p)g \sin \theta}{l(m_c+m_p \sin^2 \theta)}, f_5 = \frac{m_p l \sin \theta \dot{\theta}^2}{m_c+m_p \sin^2 \theta}, f_6 = \frac{-m_p l \dot{\theta}^2 \cos \theta \sin \theta}{l(m_c+m_p \sin^2 \theta)}$ .
- 2) Bound for  $M$ :  $|\ddot{x}| \leq |u|_{\max} + m_p l |\dot{\theta}|_{\max}^2 + \frac{m_p g}{2}, |\ddot{\theta}| \leq \frac{1}{l}(|u|_{\max} + \frac{m_p l |\dot{\theta}|_{\max}^2}{2} + (m_c + m_p)g)$  where  $|u|_{\max}$  is calculated using IBP bound.
- 3) Bound for ROA:  $\|f(x, u)\|_{\infty} = \gamma + \max(\gamma, |u|_{\max} + m_p l \gamma^2 + \frac{m_p g}{2}, \frac{1}{l}(|u|_{\max} + \frac{m_p l \gamma^2}{2} + (m_c + m_p)g))dt$ , where  $|u|_{\max}$  is the maximum force allowed.

**PVTOL** Split the region: we split the region over the domain of  $\theta$  with interval 0.25 and split the region over the domain of  $\dot{x}, \dot{y}, \dot{\theta}$  with interval 0.5. Furthermore, in the MILP we add a constraint to ensure the  $l_{\infty}$  norm of state value is no less than 0.1.

- 1) Bound for verification: we split the dynamics into three functions and bound them separately for multi-variables:  $f_1 = x \cos y, f_2 = x \sin y, f_3 = xy$ .
- 2) Bound for  $M$ : we bound each term of the dynamics with the min/max values using the monotonic property.
- 3) Bound for ROA:  $\|f(x, u)\|_{\infty} = \gamma + \max(\gamma, \gamma^2 + g + \frac{2|u|_{\max}}{m}, 2\gamma, \frac{2|u|_{\max}}{J})dt$ , where  $|u|_{\max}$  is the maximum force allowed.

## A.6. Speeding up Verification

When there is a limit on parallel resources, so that verification must be done serially for the subgrids  $k$ , we can reduce the number of grids to verify in each step as follows. The first time a verifier is called, we perform it over all subgrids; generally, only a subset will return a counterexample. Subsequently, we only verify these subgrids until none return a counterexample, and only then attempt full verification.

## A.7. ROA Calculation

For Inverted Pendulum and Path Tracking, we approximate ROA using a grid of 2000 cells along each coordinate. For Cartpole, we use a grid of 150 cells along each coordinate, and for PVTOL, we use a grid of 50 cells along each coordinate.

For benchmarks where the systems are continuous, the set levels are  $\{x \in \mathcal{R} \mid V(x) < \rho\}$  where  $\rho = \min_{x \in \partial \mathcal{R}} V(x)$ .

Note that for discrete-time systems, having  $\rho = \min_{x \in \partial \mathcal{R}} V(x)$  is not sufficient. For example, assume  $\mathcal{R}$  is the valid region, any point outside of  $\mathcal{R}$  satisfy  $V(f(x, u)) > V(x)$ , and  $\forall x \in \partial \mathcal{R}, V(x) = \rho$ . Assume we have  $x \in \mathcal{R} \setminus \partial \mathcal{R}$  and  $f(x, u) = y, y \notin \mathcal{R}$  (this is possible since the system is discrete). Since  $x$  is in the valid region, we have  $V(y) < V(x) < \rho$ . However, since  $y$  is no longer within the valid region, assume  $V(f(y, u)) > \rho > V(y)$ , the system will not converge to equilibrium point starting from point  $y$ . This means  $\{x \in \mathcal{R} \mid V(x) < \rho\}$  is not a subset of ROA.

## B. Computing Linear Bounds on Lipschitz-Continuous Dynamics

**Theorem B.1.** Given function  $g(x) : \mathbb{R}^n \mapsto \mathbb{R}$  where the Lipschitz constant is  $\lambda$ , we have  $g(x) \leq g(x_{1,l}, x_{2,l}, \dots, x_{n,l}) + \lambda \cdot \sum_i (x_i - x_{i,l})$  and  $g(x_{1,l}, x_{2,l}, \dots, x_{n,l}) - \lambda \cdot \sum_i (x_i - x_{i,l}) \leq g(x)$ , where  $x_i \in [x_{i,l}, x_{i,u}]$ ,  $\forall i \in [n]$ .

*Proof.* For any  $i \in [n]$ , given  $x_i \in [x_{i,l}, x_{i,u}]$ , for arbitrary fixed values along dimension  $[n] \setminus \{j\}$ ,

- we show that  $g(x_i, x_{-i}) \leq g(x_{i,l}, x_{-i}) + \lambda(x_i - x_{i,l})$ 
  - if  $g(x_i, x_{-i}) \geq g(x_{i,l}, x_{-i})$ , then  $g(x_i, x_{-i}) - g(x_{i,l}, x_{-i}) \leq \lambda(x_i - x_{i,l})$ , meaning  $g(x_i, x_{-i}) \leq g(x_{i,l}, x_{-i}) + \lambda(x_i - x_{i,l})$ .
  - if  $g(x_i, x_{-i}) < g(x_{i,l}, x_{-i})$ , since  $\lambda(x_i - x_{i,l}) \geq 0$ , we have  $g(x_i, x_{-i}) \leq g(x_{i,l}, x_{-i}) + \lambda(x_i - x_{i,l})$ .
- we show that  $g(x_{i,l}, x_{-i}) - \lambda(x_i - x_{i,l}) \leq g(x_i, x_{-i})$ 
  - if  $g(x_i, x_{-i}) \geq g(x_{i,l}, x_{-i})$ , then since  $-\lambda(x_i - x_{i,l}) \leq 0$ , we have  $g(x_{i,l}, x_{-i}) - \lambda(x_i - x_{i,l}) \leq g(x_i, x_{-i})$ .
  - if  $g(x_i, x_{-i}) < g(x_{i,l}, x_{-i})$ , then  $g(x_{i,l}, x_{-i}) - g(x_i, x_{-i}) \leq \lambda(x_i - x_{i,l})$ , meaning  $g(x_{i,l}, x_{-i}) - \lambda(x_i - x_{i,l}) \leq g(x_i, x_{-i})$ .

By applying the above result along all  $n$  dimensions recursively, we have the upper bound as  $g(x) \leq g(x_{1,l}, x_{2,l}, \dots, x_{n,l}) + \sum_i \lambda(x_i - x_{i,l})$ , and the lower bound as  $g(x_{1,l}, x_{2,l}, \dots, x_{n,l}) - \sum_i \lambda(x_i - x_{i,l}) \leq g(x)$ .  $\square$